GNSS-Based Phase Synchronization for Bistatic and Multistatic Synthetic Aperture Radar

Eduardo Rodrigues-Silva, Marc Rodriguez-Cassola, Gerhard Krieger, *Fellow, IEEE*, and Alberto Moreira, *Fellow, IEEE*

***Abstract*— The feasibility of single-pass interferometric or multistatic synthetic aperture radar (SAR) mission concepts largely relies on the ability to achieve the matching of the carrier phase of the different radar instruments of the constellations within a few degrees. We put forward a phase synchronization scheme in which the global navigation satellite system (GNSS) receiver and the radar payload share the same oscillator; the estimation of the synchronization phase follows from the combined evaluation of the navigation raw data and the precise orbit and baseline determination solutions. The article presents a discussion on accuracy, an error analysis, and an evaluation of its viability using a system-oriented simulation of the navigation data. The results suggest the proposed approach is capable of delivering reliable estimates of carrier frequency and phase errors for low- and medium-frequency systems in the absence of strong baseline velocity deviations if multipath and other systematic errors are successfully suppressed or calibrated.**

***Index Terms*— Bistatic radar, calibration algorithms, multistatic radar, performance analysis, time and phase synchronization.**

I. Introduction

IN BISTATIC and multistatic space radar systems, the transmitter and the receiver are spatially separated, an aspect typically associated with reduced development costs, enhanced performance, reconfigurability, and scalability [1]. In these systems, however, different oscillators are used for modulation and demodulation of the radar carrier, and the low-frequency component of the phase noise process cannot be expected to cancel out as in monostatic systems [2], [3], which will in general compromise the use of the systems for interferometric and tomographic applications [4].

As an example, the generation of digital elevation models with TerraSAR-X add-on for digital elevation measurement (TanDEM-X) required the knowledge of relative phases within a few degrees to avoid systematic modulations in the interferometric measurements [5]. In that case, synchronization with that level of accuracy was achieved by exchanging pulses at the radar carrier frequency between the satellites through a direct microwave link [6], which involved the implementation of six horn antennas connected to the radar payload, covering most of the angular environment of the satellites. Besides the need for additional hardware, the incorporation of such direct links may be problematic due to differences in the development schedules of different elements of the constellation, as it is typically the case of companion synthetic aperture radar (SAR) missions [7].

In a full system architecture (e.g., MirrorSAR, [8], [9]), it is envisaged to avoid the demodulation of the radar signals by having the receivers act like transponders, i.e., rerouting the radar echoes to another element of the constellation (e.g., the transmitter) having access to the oscillator used in the modulation. Although a MirrorSAR architecture requires a direct link between the satellites, not necessarily in the microwave range, it still keeps the potential for relevant spacecraft simplification by the possible removal of complete hardware blocks for demodulation, data storage, downlink, or digital control in the receivers.

The estimation of the synchronization phase is based on the evaluation of the received data (e.g., autosync), though demonstrated in spaceborne environments [10], [11], provides estimates with varying quality as a function of the backscattering of the scene, which can only be arguably acceptable as a baseline solution for interferometric SAR missions.

In [12] a synchronization scheme for bistatic and multistatic radar based on global positioning system (GPS) is proposed, where the transmitter and the receiver in different platforms use an ultrastable oscillator (USO) disciplined by the output pulse-per-second (PPS) signal generated by the embedded GPS receiver. It combines the advantages of the good short-term stability of high-quality USO with the long-term stability of the PPS signal generated by the GPS receiver. The technique, however, relies largely on the evaluation of the received data to compensate for time fluctuations of the PPS signal and the short-term phase variations of the USO.

We put forward in this article an approach to estimate the oscillator phase errors in bistatic and multistatic SARs based on the coherent evaluation of navigation data from the global navigation satellite system (GNSS) receivers on transmitting and receiving satellites and the baseline solution obtained via precise orbit determination (POD), provided both the radar and the navigation receivers share the same primary oscillator. We exploit the fact that the phase drift of the oscillator in the navigation receiver can be estimated in the standard navigation solution. This drift directly affects the pseudorange measurements between the GNSS satellites and the GNSS receivers and is estimated along with the position and velocity in a filter. In principle, only the raw data of the GNSS receivers at the highest possible rate is required for the

Manuscript received 17 October 2023; revised 10 March 2024; accepted 17 May 2024. Date of publication 28 May 2024; date of current version 10 June 2024. This work was supported by the German Academic Exchange Service (DAAD) under Grant 57540125. *(Corresponding author: Eduardo Rodrigues-Silva.)*

The authors are with the Microwaves and Radar Institute of the German Aerospace Center (DLR), 82234 Weßling, Germany (e-mail: eduardo.rodriguessilvafilho@dlr.de).

Digital Object Identifier 10.1109/TGRS.2024.3406797

complete duration of the SAR acquisition period. Since the raw data of the GNSS receivers of the two spacecraft need be available for the estimation of the synchronization solution, the technique is better suited for implementation on ground to be used during the calibration and processing stages of the bistatic and multistatic data.

The suggested approach links the synchronization and navigation solutions, i.e., accurate baseline determination, which is a *sine qua non* condition for its successful operation. This commonality, hardly new in the context of bistatic and multistatic SAR, is shared with the solution of a simplex synchronization link, the original MirrorSAR architecture, and interferometric autosync implementations.

The capability of high-accuracy relative positioning (i.e., baseline determination) using GNSS has been extensively demonstrated in space. In the gravity recovery and climate experiment (GRACE) mission, an accuracy of 1 mm compared to a K-band ranging system [13] was reported. TanDEM-X achieved accuracy in the order of 1-2 mm through a posteriori calibration based on the evaluation of the raw topographic maps acquired under different geometries [14]. Both missions used geodetic GPS receivers, capable of receiving two frequencies for correcting the effects of the ionosphere. The prototype research instruments and space mission technology advancement (PRISMA) mission, on the other hand, demonstrated the capability of achieving subdecimeter relative positioning precision using a low-cost single-frequency GPS receiver [15]. An associated capability for high-accuracy relative timing can be inferred from the dependency between time and position accuracy in GNSS-based POD.

Our suggested solution indicates that it is capable of capable of providing reliable estimates of the oscillator synchronization phase, biased by the absolute baseline error, up to frequencies beyond the X-band provided the contributions of the baseline velocity error, differential ionospheric delays, multipath, and other systematic components are negligible or calibrated. The results show that the technique could be used to achieve relative phase synchronization. Its ability to provide absolute phase synchronization depends on the precision to which all the biases can be calibrated, e.g., by means of a posteriori evaluating of the raw topographic maps acquired under different geometries. The article presents a detailed analysis of the phase synchronization accuracy and the impact of all systematic components on the solution.

Section II presents the impact of the lack of synchronization on bistatic SAR images. Section III describes a simple model for the synchronization solution based on the evaluation of POD and GNSS data. Section IV presents an error analysis, detailing all the factors that affect the precision of the phase estimation. Section V validates the analysis employing an end-to-end simulation and discusses its usability and performance in a representative scenario. Section VI closes the article with a conclusion and general discussion.

II. Impact of Lack of Synchronization in Bistatic SAR

The phase error introduced by the operation with different oscillators in bistatic SAR data is proportional to the difference in primary oscillator phase output between the transmitter and the receiver [2], [3] as follows:

$$\psi_{\text{clock}}(t) = \psi_{0,\text{clock}} + 2\pi \cdot \int_{t_0}^{t} \mathrm{d}\tau \cdot \delta f_{\text{clock}}(\tau) \tag{1}$$

where t is the time, $\psi_{0,\text{clock}}$ is a constant not relevant for the analysis, and $\delta f_{0,\text{clock}}$ is a random process representing the instantaneous difference in the radar carrier of the transmitter and the receiver. The term δf_{clock} can be further expressed as a constant carrier offset $\delta f_{0,\text{clock}}$ and a zero-mean random process $\delta f_{\text{st,clock}}$ as follows:

$$\delta f_{\text{clock}}(t) = \delta f_{0,\text{clock}} + \delta f_{\text{st,clock}}(t)\,. \tag{2}$$

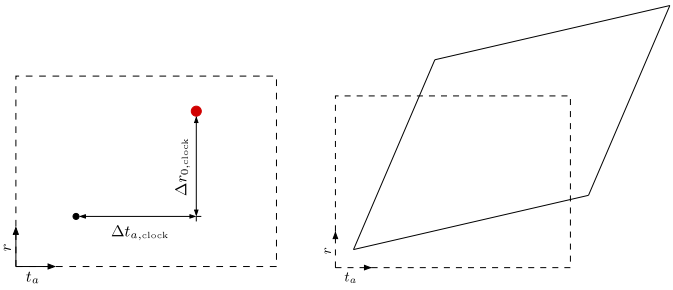

Fig. 1. Effect of differential clock errors on (left) the focused targets and on (right) the focused image assuming positive $\delta f_{0,\text{clock}}$. The difference in color represents the different phase of the point target.

Fig. 1 illustrates the rough effect of the clock error on a focused point target (left) and on the focused image (right). The focused point target suffers 2-D positioning errors, slight defocusing, and interferometric phase errors, represented by the color change in the left image. The focused image suffers a distortion in range and azimuth roughly proportional to the carrier offset between transmitter and receiver, as well as a bulk range offset due to the uncertainty in the bistatic time reference, as shown in the right drawing.

III. GNSS-Based Synchronization Approach

Fig. 2 shows the block diagram of a possible system implementation of the suggested approach. In the figure and throughout this article, t denotes the GPS time, and all variables are expressed in the international celestial reference frame (ICRF). Without loss of generality, the measurement models do not take into account relativistic effects.[1]

In the proposed architecture, the same USO is used for generating the radar carrier and the reference signal in the GNSS receiver. Please note the GNSS receiver must be able to switch its reference to an external oscillator, a feature in some space-qualified receivers (e.g., Beyond Gravity PODRIX used in Sentinel-1). The carrier phase single-differences between the two spacecraft then will contain information on the phase noise difference between the oscillators at the different

[1]The SAR processing equations and geometry are described in an Earth-centered Earth-fixed frame (ECEF), resulting in a nonsimultaneity effect between the two frames which may cause considerable time, phase, and frequency deviations, which are larger the longer the baseline is [16]. These effects are deterministic and can be calculated and compensated in the data processing. For more details on the relativistic effects on GNSS measurements, please refer to [17]. Details on the relativistic effects on SAR processing are given in [16].

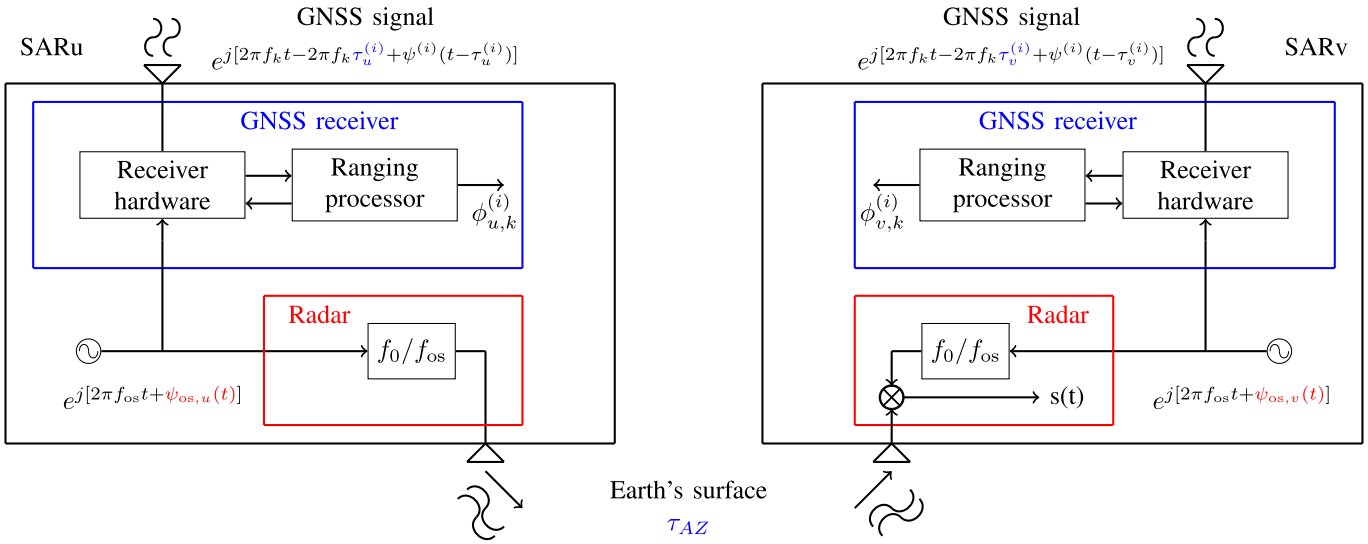

Fig. 2. Proposed hardware configuration for radar phase synchronization based on GNSS, also used as the basis for the analysis. In this figure, $\tau_{(u,v)}^{(i)}$ are the delays from GNSS satellite i to the SAR satellites.

platforms measured at the navigation carriers. The suggested approach is based on the assumption that this measurement will provide, after appropriate calibration and scaling, a good estimation of the phase difference between the two radar carriers.

A. Signal Model

In the following equations, we denote the upper index $()^{(i)}$ as relating to the GNSS satellite i, the lower indexes $()_u$ and $()_v$ as relating to the receivers in the satellites u and v, and the lower index followed by a comma, as in $()_{u,k}$, as related to the reference frequency, with navigation carrier frequency denoted by k, the oscillator nominal frequency by os, and the radar carrier by 0. Furthermore, we denote the difference between quantities as $()_{uv} = ()_v - ()_u$.

Under the assumption of ideal upconversion stages, the phases of the radar reference signal $\psi_{u,0}$ and the phase of the primary oscillator input of the GNSS receiver clock $\psi_{u,\mathrm{os}}$ are related as follows:

$$\psi_{u,0}(t) = \psi_{bu,0} + \frac{f_0}{f_{\mathrm{os}}} \cdot \psi_{u,\mathrm{os}}(t) \tag{3}$$

where $\psi_{bu,0}$ is a phase bias, f_0 is the nominal carrier frequency of the radar, and f_{os} is the nominal frequency of the primary oscillator. Equation (3) suggests any phase drift in the output of the primary oscillator will be replicated in all reference signals derived from it, only scaled by the appropriate upscaling or downscaling factors. This assumption requires the spectral purity of the upconverting stages in the radar electronics, to be further elaborated in Section IV. Furthermore, we can assume that the clock biases of the receivers ideally hold a linear dependency with the phase of the primary oscillator, which can be expressed in the following equations:

$$\delta t_u(t) = \delta t_{0u} + \frac{1}{2\pi \cdot f_{\mathrm{os}}} \cdot \left[\psi_{u,\mathrm{os}}(t) - \psi_{u,\mathrm{os}}(t_{0u})\right] \tag{4}$$

$$\delta t_v(t) = \delta t_{0v} + \frac{1}{2\pi \cdot f_{\mathrm{os}}} \cdot \left[\psi_{v,\mathrm{os}}(t) - \psi_{v,\mathrm{os}}(t_{0u})\right] \tag{5}$$

where $\delta t_\star$ are the clock biases, $\delta t_{0\star}$ is the initialization times difference, and $\psi_{\star,\mathrm{os}}(t_{0\star})$ are the oscillator phases at initialization. In that case, the differential time offset between clocks is given by

$$\delta t_{uv}(t) = \delta t_{0uv} + \frac{\psi_{uv,\mathrm{os}}(t)}{2\pi \cdot f_{\mathrm{os}}} \tag{6}$$

where

$$\delta t_{0uv} = \delta t_{0v} - \delta t_{0u} - \frac{1}{2\pi \cdot f_{\mathrm{os}}} \cdot \left[\psi_{v,\mathrm{os}}(t_{0v}) - \psi_{u,\mathrm{os}}(t_{0u})\right]. \tag{7}$$

Equation (6) suggests that the differential phase drift of the primary oscillator can be recovered from the difference between receiver clock biases, assuming the linear dependencies between phase and clock bias expressed in (4) and (5) are valid.

The phase of the primary oscillator at each receiver $\psi_{u,\mathrm{os}}(t)$ and $\psi_{v,\mathrm{os}}(t)$ can be decomposed into a linear component due to a constant frequency $f_\star$, a random process $\phi_\star(t)$, and a constant offset $\phi_{\star 0}$ as follows:

$$\psi_{u,\mathrm{os}}(t) = 2\pi \cdot f_u \cdot t + \phi_u(t) + \phi_{u0} \tag{8}$$

$$\psi_{v,\mathrm{os}}(t) = 2\pi \cdot f_v \cdot t + \phi_v(t) + \phi_{v0}. \tag{9}$$

Note that the phase noise affecting the bistatic radar measurements is the scaled version of the differences between the transmitter and receiver oscillators evaluated at times delayed by τ_{AZ}, the two-way travel time of the radar signals, as acknowledged in [4]. This lag, typically in the order of milliseconds, is beyond the inverse of the bandwidth relevant to the calibration of the bistatic SAR data, which allows us to approximate

$$\phi_v(t - \tau_{\mathrm{AZ}}) - \phi_u(t) \approx \phi_v(t) - \phi_u(t). \tag{10}$$

B. Estimation of the Synchronization Phase

The proposed estimator is illustrated in Fig. 3. The idea is to calibrate the systematic components present in the single

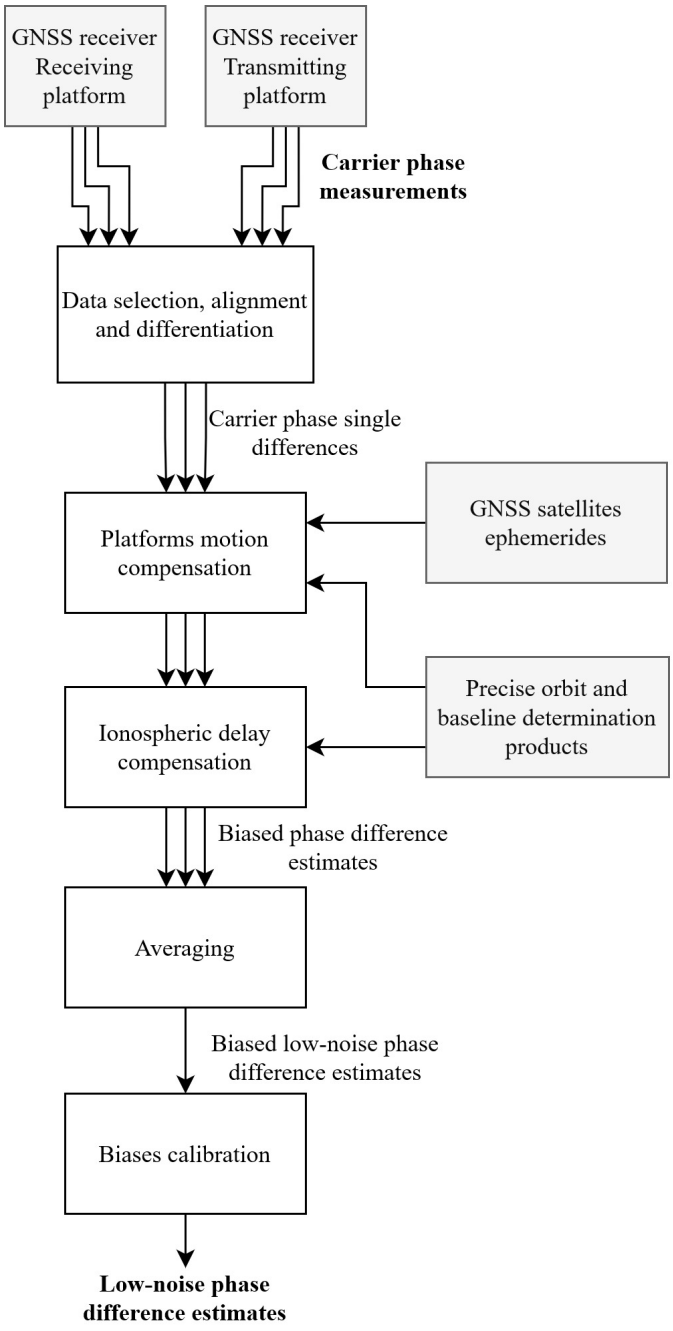

Fig. 3. Proposed GNSS-based estimator of radar carriers phase difference.

differences of the carrier phases using the information on the baseline, ambiguities, and bulk ionospheric delays derived from precise orbit and baseline determination.

The differential phase noise of the oscillators on the two satellites could be extracted from the single differences in case the other factors can be determined with sufficient accuracy by other means. In that case, we would obtain estimates of the differential phase noise at the sampling rate of the carrier phase measurements. The differential signal path length and ionospheric delay can be determined with high accuracy from the POD process. The residual error from the POD process varies at different time scales as the phase noise error, which makes it possible to separate the two, as will be explained in detail in Section IV-B.

The complete estimation (i.e., POD and clock phase) could also be done in a single step, in which both the baseline and clock phase differences are estimated simultaneously. We stick in this article to the two-step solution for the sake of simplicity of the analysis. The single-step approach is not expected to improve noticeably the accuracy of the estimation due to the different temporal scales of the clock phase noise (with much faster variations) and the changes in spacecraft acceleration (much slower).[2] It is important to mention that since the same oscillator is used for the radar and GNSS receiver, it has to satisfy constraints for both systems.

A biased measurement of the distance between the GNSS receiver and the GNSS satellite can be derived from the code delay or the carrier phase measurement. The former is unambiguous but associated with lower precision, typically about two orders of magnitude. The relationship between the differential carrier phase measurements $L_{uv,k}^{(i)}$—here directly scaled by a factor $\lambda_k/2\pi$ and therefore expressed in units of meters—and the clock biases expressed in time δt_{uv} is given by [19]

$$L_{uv,k}^{(i)}(t) = \rho_{uv}^{(i)}(t) + c \cdot \delta t_{uv}(t) - \left(\frac{\lambda_k}{\lambda_1}\right)^2 \cdot I_{uv}^{(i)}(t) - \lambda_k \cdot A_{uv,k}^{(i)} + M_{uv,k}^{(i)}(t) + \epsilon_{uv,k}^{(i)}(t) \quad (11)$$

where $\rho_{uv}^{(i)}$ is the difference between the distances from receivers v and u to the ith navigation satellite, respectively, c is the speed of light in vacuum, $I_{uv}^{(i)}$ is the difference between the biases caused by the ionospheric delays for a signal at wavelength λ_1, $A_{uv,k}^{(i)}$ is the ambiguity difference, $M_{uv}^{(i)}(t)$ describes other systematic error components including multipath, crosstalk, tracking channel bias, and phase wind-up, and $\epsilon_{uv}^{(i)}(t)$ is a thermal noise process. Substituting from (6) and (3), we can identify the relationship between navigation data and the clock synchronization solution as follows:

$$\frac{\lambda_0}{2\pi} \cdot \psi_{uv,0}(t) = L_{uv,k}^{(i)}(t) + \lambda_k \cdot A_{uv,k}^{(i)} - \rho_{uv}^{(i)}(t) + \left(\frac{\lambda_k}{\lambda_1}\right)^2 \cdot I_{uv}^{(i)}(t) + \frac{\lambda_0}{2\pi} \cdot \psi_{buv,0} - c \cdot \delta t_{0uv} - M_{uv,k}^{(i)}(t) - \epsilon_{uv,k}^{(i)}(t). \quad (12)$$

An estimator of the clock synchronization solution using a weighted average over all navigation satellites in sight (i.e., N) and all the $n_\lambda^{(i)}$ received GNSS frequencies can be straightforwardly derived as

$$\tilde{\psi}_{uv,0} = \frac{2\pi}{\lambda_0} \cdot \sum_{i=1}^{N} \sum_{k=1}^{n_\lambda^{(i)}} \alpha_k^{(i)} \cdot \left[L_{uv,k}^{(i)} + \lambda_k \cdot \tilde{A}_{uv,k}^{(i)} - \tilde{\rho}_{uv}^{(i)} + \left(\frac{\lambda_k}{\lambda_1}\right)^2 \cdot \tilde{I}_{uv}^{(i)} \right] + \tilde{\psi}_{buv,0} - \frac{2\pi \cdot c}{\lambda_0} \cdot \delta\tilde{t}_{0uv} \quad (13)$$

[2] See [18] for an example in which a higher sampling rate does not improve the precision of the navigation solution.

where $\tilde{\cdot}$ indicates the POD estimate for all the terms and $\alpha_k^{(i)}$ are the weights for the signal from each navigation satellite according to its quality (e.g., signal-to-noise ratio), with the sum of $\alpha_k^{(i)}$ being equal to one. Note that the terms in the second sum have been assumed to be sampled according to the condition in (10). Equation (13) provides an unbiased estimation under the assumption that $M_{uv,k}^{(i)}$ is negligible, $\epsilon_{uv,k}^{(i)}$ is a zero-mean process, and no relevant biases are introduced in the baseline determination process. As hinted earlier, the term under the summation contains systematic error components which may, if not properly removed, bias the resulting estimates.

Assuming the measurements are statistically independent Gaussian processes, the value of $\alpha_k^{(i)}$ which minimizes the variance of the estimator is given by

$$\alpha_k^{(i)} = \frac{\left(\sigma_k^{(i)}\right)^{-2}}{\sum_{i=1}^{N}\sum_{j=1}^{n_\lambda^{(i)}}\left(\sigma_j^{(i)}\right)^{-2}} \tag{14}$$

where the $\sigma_k^{(i)}$ correspond to the standard deviation of the measurements (e.g., of the residuals of the POD). A sensible assumption for the derivation of the estimator performance is: 1) a successful calibration of relevant systematic components and 2) the measurement is dominated by thermal noise in the receiver. Under these circumstances, for a phase-locked loop (PLL) discriminator, $\sigma_k^{(i)}$ can be expressed as a function of the carrier-to-noise ratio $(c/n_0)_k^{(i)}$ as follows:

$$\sigma_k^{(i)} \approx \sqrt{\frac{B_{\mathrm{L-CA}}}{(c/n_0)_k^{(i)}}} \tag{15}$$

where $B_{\mathrm{L-CA}}$ is the so-called tracking bandwidth of the GNSS receiver [20]. Substituting (15) into (16), we get

$$\alpha_k^{(i)} = \frac{(c/n_0)_k^{(i)}}{\sum_{i=1}^{N}\sum_{j=1}^{n_\lambda^{(i)}}(c/n_0)_j^{(i)}} \tag{16}$$

where the (c/n_0) values provided by the GNSS receiver can be used. Note that these values may change during the data acquisition period, which would result in time-varying weights $\alpha_k^{(i)}$. In case the individual phase error estimates are biased, this variation would cause undesirable dynamic error components. Therefore, we recommend fixing the values of $\alpha_k^{(i)}$ for the whole data acquisition period by using, for example, an average of the (c/n_0) measurements.

IV. Error Analysis

A further elaboration of the system model suggests the incorporation of other systematic phase signatures occurring in the radar and navigation receiver electronics, which might not be assumed to be uncorrelated for different navigation frequencies. Under these circumstances, we can relate the phase differences at radar and navigation carriers between the two satellites with the relative clock bias as follows:

$$\delta t_{uv}(t) = \delta t_{0uv} + \frac{1}{2\pi \cdot f_0}\cdot\left[\psi_{uv,0}(t) + \delta\psi_{\mathrm{HW}uv,0}(t)\right] \tag{17}$$

where $\delta\psi_{\mathrm{HW}uv,0}$ denotes the residual signature caused by radar and navigation receiver hardware.

The error in the estimation of the differential phase at the radar carrier can be derived after combining (13), (11), and (17) as follows:

$$\begin{aligned}
&\delta\psi_{uv,0}(t)\\
&= \sum_{i=1}^{N}\sum_{k=1}^{n_\lambda^{(i)}}\frac{2\pi}{\lambda_0}\cdot\alpha_k^{(i)}\\
&\quad\cdot\left\{\tilde{\rho}_{uv}^{(i)}(t) - \rho_{uv}^{(i)}(t) - \epsilon_{uv,k}^{(i)}(t)\right.\\
&\qquad - M_{uv,k}^{(i)}(t) + \left(\frac{\lambda_k}{\lambda_1}\right)^2\cdot\left[I_{uv}^{(i)}(t) - \tilde{I}_{uv}^{(i)}(t)\right]\\
&\qquad \left.+\lambda_k\cdot\left(A_{uv,k}^{(i)} - \tilde{A}_{uv,k}^{(i)}\right)\right\} + \psi_{buv,0} - \tilde{\psi}_{buv,0}\\
&\qquad - \frac{2\pi\cdot c}{\lambda_0}\cdot\left(\delta t_{0uv} - \delta\tilde{t}_{0uv}\right) - \delta\psi_{\mathrm{HW}uv,0}(t).
\end{aligned} \tag{18}$$

Equation (18) describes the error in the estimation of the phase difference between the two primary oscillators at the radar carrier frequency. Since the error components are proportional to the inverse of the radar wavelength, the estimation error is expected to increase for higher radar frequencies. We discuss in Sections IV-A–IV-G in more detail the impact of the error terms in (18).

A. Thermal Noise

The thermal noise contribution describes the boundary of the performance of the algorithm in the absence of the other systematic components. Under the assumption of statistical independence and identical noise power for all frequencies corresponding to the measurement of a given navigation satellite, we can express the standard deviation of the phase estimator due to thermal noise as

$$\sigma_\epsilon = \frac{2\pi}{\lambda_0}\cdot\sqrt{\sum_{i=1}^{N}\frac{\alpha_i^2\cdot\sigma_{uv,i}^2}{n_\lambda^{(i)}}} \tag{19}$$

where $\sigma_{uv,i}$ is the standard deviation of the differential noise process corresponding to the signal received from the navigation satellite i. Under the assumption that both parts receive the signals of satellite i with similar quality, quite reasonable for standard baselines and equal GNSS receivers, and substituting from (16), the previous expression may be approximated as

$$\sigma_\epsilon \approx \frac{2\pi}{\lambda_0}\cdot\sqrt{\frac{2}{n_\lambda}\cdot\frac{1}{\sum_{i=1}^{N}\sigma_i^{-2}}} \tag{20}$$

where the same number of available navigation frequencies n_λ for all satellites has been assumed. As expected, the accuracy of the estimation improves with an increasing number of satellites and frequencies tracked. The noise boundary for the performance of the GNSS-based estimation of the synchronization phase can be expressed as

$$\sigma_\psi = \sigma_\epsilon\cdot\sqrt{\frac{B_\psi}{f_{\mathrm{GNSS}}}} \approx \frac{2\pi}{\lambda_0}\cdot\sqrt{\frac{2\cdot B_\psi}{n_\lambda\cdot f_{\mathrm{GNSS}}}\cdot\frac{1}{\sum_{i=1}^{N}\sigma_i^{-2}}} \tag{21}$$

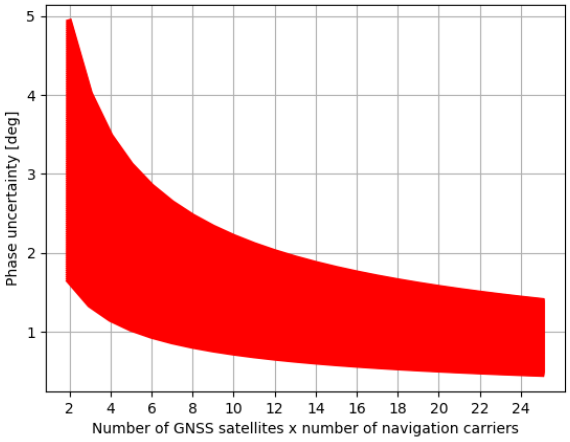

Fig. 4. Phase noise accuracy according to the model in (21) for a 5.405 GHz SAR payload (e.g., Sentinel-1 carrier phase), with the number of satellites in view N varying from 2 to 12 and the number of frequencies n_λ up to two. The standard deviation in ranging caused by thermal noise has been assumed to vary between 1.2 and 0.4 mm, values consistent with the technical specification of the Phoenix receiver of DLR. The final phase uncertainty depends on the standard deviation of the individual satellites, but in this example would be necessarily within the shaded region.

TABLE I
SIMULATION PARAMETERS FOR PHASE UNCERTAINTY CALCULATION

Parameter	Value
Radar carrier frequency [GHz]	5.405
Thermal ranging accuracy [mm]	[0.4, 1.2]
Number of GNSS satellites	[2, 12]
n_λ	[1, 2]
B_ψ [Hz]	2
f_{gnss} [Hz]	5

where B_ψ represents the bandwidth of the oscillator phase noise relevant for the correction of the bistatic SAR data and f_{GNSS} corresponds to the rate at which the pseudoranges are made available by the GNSS receivers. The value of B_ψ depends on the characteristics of the primary oscillator and the carrier frequency of the radar; for interferometric applications, typical values for B_ψ are in the order of a few (e.g., less than ten) Hz. In the case of TanDEM-X, the direct link is operated at a rate of 5 Hz, a value consistent with the performance estimation reported in [5].

Fig. 4 shows an example of the expected contribution of the thermal noise performance in terms of noise for the proposed GNSS-based synchronization scheme in the case of a 5.405 GHz SAR payload.[3] The receiver performance is based on the single-frequency GPS receiver Phoenix developed by the German Space Operations Center (GSOC) of DLR [21], but with the assumption of dual-frequency operation with similar accuracy on both navigation carriers. The specific values of the simulation are listed in Table I.

B. Baseline Errors

As suggested by (18), baseline estimation errors directly appear as residual phase signatures in the estimated solutions. The baseline error term in (18) can be decomposed as the superposition of the baseline error in the navigation solution and the error in the transformation from the phase center of the navigation to the radar antennas. The latter can be assumed to be negligible in typical orbital scenarios.

The error in the baseline determination depends on how the real baseline changes over time compared to the estimated baseline. The PRISMA mission provides some useful figures for assessing the shape and magnitude of this error. In an initial phase, the two spacecraft were physically attached, which allowed for an independent, highly accurate, estimate of the baseline using the attitude information [15]. The differences between the two estimates in radial, along-track, and across-track components describe, most of the time, a sinus-like shape over an orbital period with amplitudes of a few millimeters. This suggests that the baseline can be approximated in close formation scenarios by a linear term for acquisitions of several minutes. The PRISMA data show, however, some discontinuities that should be avoided in the estimates used for the derivation of the synchronization solution.

Linear baseline errors will be interpreted by the clock synchronization solution as carrier offset. In the case of interferometric applications on static surfaces, the resulting carrier offset can be easily estimated in the data processing if it is constant over scales of a few minutes [11]. For other applications, the carrier offset would result in artifacts on the synthesized image, so the applicability of the synchronization technique here proposed is tied to the baseline velocity precision. This could be particularly problematic for moving surface applications.

The carrier offset due to baseline velocity errors is, however, expected to be very low. Consider, for example, a 5.405 GHz SAR payload. Based on (23), which will be derived shortly, a baseline velocity error of 0.008 mm/s in the radial direction-loosely based on results from PRISMA mission [15]-and a radial component of the GNSS-SAR average direction vector of -0.6 would result in a carrier offset of about 0.086 mHz. In the case of the interferometric SAR systems, any residual ramp can be easily estimated from data acquired over land areas [10], [11].

In the following paragraphs, we derive an approximate explicit relation between the baseline and phase synchronization errors to provide further insight into its impact. The baseline determination error for each GNSS satellite can be approximated as follows by linearizing the error term around zero as a function of the baseline solution [19]:

$$\rho_{uv}^{(i)} - \tilde{\rho}_{uv}^{(i)} \approx -\tilde{\vec{e}}_v^{(i)} \cdot \Delta\vec{r}_{uv} - \tilde{\vec{e}}_{uv}^{(i)} \cdot \Delta\vec{r}_u + \tilde{\vec{e}}_{uv}^{(i)} \cdot \Delta\vec{r}^{(i)} \quad (22)$$

in which the $\tilde{\vec{e}}_u^{(i)}$ are unit vectors in the direction from the estimated position of SAR satellite u to GNSS satellite i, $\Delta\vec{r}^{(i)}$ is the error in the position of GNSS satellite i, $\Delta\vec{r}_{uv}$ is the baseline error, and $\Delta\vec{r}_u$ is the error in the position of SAR satellite u, as shown in Fig. 5. For baselines up to a few kilometers, the vectors $\tilde{\vec{e}}_u^{(i)}$ and $\tilde{\vec{e}}_v^{(i)}$ are approximately parallel and the terms $\tilde{\vec{e}}_{uv}^{(i)} \cdot \Delta\vec{r}_u$, and $\tilde{\vec{e}}_{uv}^{(i)} \cdot \Delta\vec{r}^{(i)}$ are small compared to the first term in the equation. In that case, we can approximate the individual orbit determination errors as the

[3]The simulated case corresponds to that of a bistatic companion of ESA's Sentinel-1 satellite and has been used by the authors as a reference for the ESA Earth Explorer 10 mission Harmony.

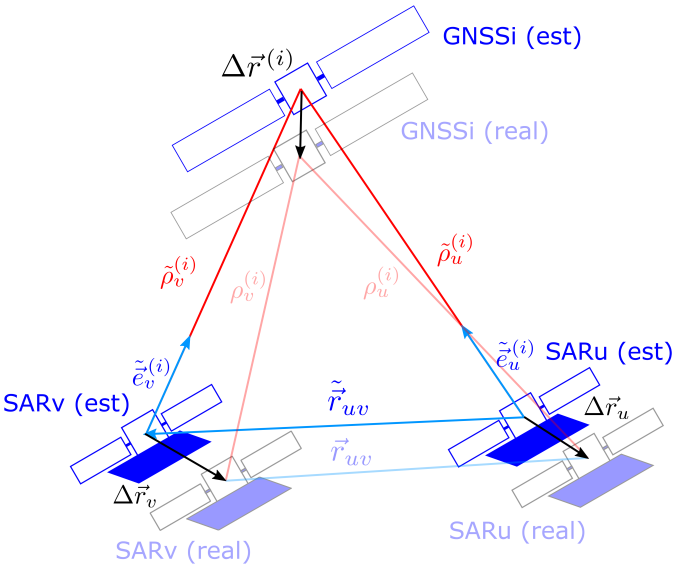

Fig. 5. Basic geometry for the derivation of the baseline determination error.

first term of (22), i.e.,

$$\sum_{i=1}^{N}\sum_{j=1}^{n_\lambda^{(i)}}\alpha_k^{(i)}\cdot\left[\rho_{uv}^{(i)}(t)-\tilde{\rho}_{uv}^{(i)}(t)\right]\approx\Delta\vec{r}_{vu}(t)\cdot\sum_{i=1}^{N}\alpha_i\cdot\tilde{\vec{e}}_v^{(i)}(t) \tag{23}$$

with

$$\alpha_i=\sum_{k=1}^{n_\lambda^{(i)}}\alpha_k^{(i)}.$$

The summation on the right corresponds to a weighted average of unit vectors distributed more or less uniformly in a semi-sphere. Since the weights α_i depend on the signal-to-noise ratio, higher elevations will receive a higher weight. Assuming an antenna pattern symmetrical with respect to the direction of the main lobe, the terms in the along-track and across-track in the individual vectors $\tilde{\vec{e}}_v^{(i)}$ will tend to cancel out when taking the average. These two factors contribute to making this summation term a vector predominantly in the radial direction. Since the final result is the scalar product of the baseline error with this roughly radial vector, the radial component of the baseline error will tend to dominate the final error in the baseline estimation.

Fig. 6 illustrates the influence of each component of the baseline error in the phase synchronization solution. It corresponds to the application of (23) to simulated orbital data considering a 5.405 GHz SAR payload. The GNSS orbits are obtained from propagated GPS two-line elements (TLEs) data. It gives an idea of the order of magnitude and structure resulting from the baseline error and corroborates the higher influence of the radial component. Note the plot shows the behavior of the error over a period of hours. Within the temporal scales of the synthetic aperture or SAR acquisitions-typically a few minutes-, the observed variations remain negligible (e.g., below one second of arc per millimeter for 1 min). For a modest baseline accuracy of about 1-2 cm, the static baseline contribution as shown in Fig. 6 would be

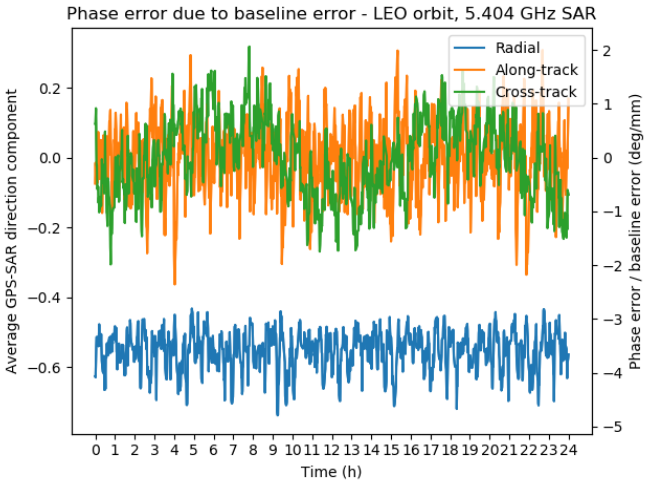

Fig. 6. Components of the GNSS-SAR average direction vector for a 500 km altitude circular orbit and expected phase estimation error per millimeter baseline error for a 5.405 GHz SAR payload.

tens of degrees in total, and the dynamic synchronization error could become significant.

C. Residual Signatures of the Receiver and Upconverting Electronics

The model in (3) assumes the ideal behavior and spectral purity of all upconverting and frequency synthesizer electronics in transmitter and receiver, a *sine qua non* for the scaling of the phase noise process measured using the navigation data onto the radar carrier. The residual signature considered in (17) is expected to contaminate the solution if any of the previous conditions are not satisfied. The averaging of the error due to residual signatures in the upconverting electronics can be-at best-only expected to happen over the few navigation carriers of the receiver, if at all. This error source is common for all received signals, and therefore cannot be reduced by averaging the measurements from different frequencies and GNSS satellites. It corresponds to a performance floor of the synchronization technique here presented.

The receiver may use PLLs to lock local oscillators-used for downconversion of the received signal-to the primary oscillator, and a digitally controlled oscillator (DCO) to generate the internal reference signal [20]. A PLL could also be used to lock an internal oscillator to an external frequency source. The jitter added by these frequency generation devices within the receiver is expected to cause a deviation from the ideal proportionality between the clock term of the carrier phase measurement, and the phase noise of the primary oscillator, adding to the residual signature.

Among the many architectural implications of the conditions above (e.g., low-phase noise of mixers, PLLs, and other active elements especially in the navigation receivers), we believe it is pertinent to focus on the selection of the primary frequency of the system. Above all, the use of other oscillators only impacting either the navigation receiver or the radar electronics should be avoided. If the use of frequency shifts cannot be avoided or other relevant nonlinearities are expected in the navigation receivers, it may be advisable to sample the primary oscillator of the system (and other

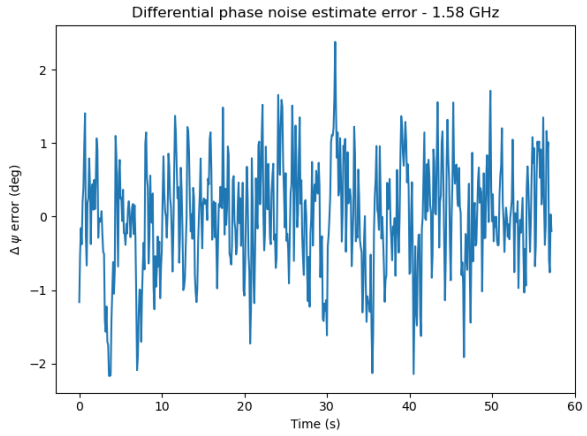

Fig. 7. Measured error of smoothed carrier differential phase noise estimates using two OEM729 receivers with a common external frequency source in a zero-baseline configuration. The carrier phase data was taken at 10 Hz and smoothed through a moving average with a window size of ten samples.

intermediate frequencies) to provide a reference for further calibration of the synchronization solution.

The performance floor contribution from receiver electronics, added to the carrier phase tracking error due to thermal noise, can be determined by calculating the single differences of the carrier phase measurements between two receivers taking as input the same GNSS signal (e.g., using the same antenna) and the same primary oscillator. Results from such experiments are reported in [22]. In the article, the authors show that a performance floor of 1 mm rms in the L1 band, which corresponds to 1.9°, is achievable with currently available dual-frequency geodetic-grade receivers.

We executed an experimental validation using two of the receivers OEM729 from Novatel, configured to receive signals from the GPS constellation only. In the experiment, the two receivers are configured to use an external frequency source, and share the same oscillator signal and the same antenna, therefore emulating a perfect baseline determination. The results are shown in Fig. 7. The figure shows the average of eight tracked L1 carrier phases, subtracted from the constant bias and smoothed using a moving average filter of ten samples, which corresponds to 1 s of data. The figure shows results that may be sufficient for an L-Band system, indicating that sufficient accuracy for lower frequency SAR systems could also be attained by conventional receivers. We believe it is possible to design receivers fulfilling the requirement of having negligible, or at least traceable, clock signatures added to the oscillator phase noise. In that case, performance in phase synchronization would be driven by thermal noise and POD accuracy.

This article is focused on the error sources over which the receiver and radar payload designers have little control. The simulation presented in Section V assumes that the performance floor established by the receiver and radar electronics is well below the thermal noise component at the tracking loop of each signal.

D. Ionospheric Delay

As mentioned before, the ionospheric delays can be estimated in the POD along with the clock bias, position, and other parameters. For short baselines, of less than one kilometer, ionospheric path delays for the two satellites are expected to be highly correlated. For example, in the GRACE mission, the differential path delays were dominated by carrier phase measurement noise, which resulted in a scatter of roughly 1 cm [23]. The differential ionospheric delay thus is expected to be very low and the error from the differential ionospheric delay estimation is expected to be even lower.

In case the differential ionospheric delay component is not negligible, it can be directly eliminated by employing a dual-frequency receiver. From (12), the observables from a dual-frequency receiver can be modeled as

$$\frac{\lambda_0}{2\pi}\cdot\psi_{uv,0}-I_{uv}^{(i)}=P_{Luv,1}^{(i)}-\rho_{uv}^{(i)}-c\cdot\delta t_{0uv}-\epsilon_{uv,1}^{(i)} \tag{24}$$

$$\frac{\lambda_0}{2\pi}\cdot\psi_{uv,0}-\left(\frac{\lambda_k}{\lambda_1}\right)^2\cdot I_{uv}^{(i)}=P_{Luv,2}^{(i)}-\rho_{uv}^{(i)}-c\cdot\delta t_{0uv}-\epsilon_{uv,2}^{(i)}. \tag{25}$$

We can isolate the phase error from the system of equations above, which results in

$$\psi_{uv,0}=\frac{2\pi}{\lambda_0}\cdot\left(\frac{\lambda_2^2}{\lambda_2^2-\lambda_1^2}\right)\cdot\left[P_{Luv,1}^{(i)}-\left(\frac{\lambda_1}{\lambda_2}\right)^2\cdot P_{Luv,2}^{(i)}-\left(1-\frac{\lambda_1^2}{\lambda_2^2}\right)\cdot\rho_{uv}^{(i)}\right]-\frac{2\pi\cdot c}{\lambda_0}\cdot\delta t_{0uv}+\epsilon_{uv,12}^{(i)} \tag{26}$$

where

$$\epsilon_{uv,12}^{(i)}=\frac{2\pi}{\lambda_0}\cdot\left(\frac{\lambda_2^2}{\lambda_2^2-\lambda_1^2}\right)\cdot\left(\epsilon_{uv,1}^{(i)}+\frac{\lambda_1^2}{\lambda_2^2}\cdot\epsilon_{uv,2}^{(i)}\right). \tag{27}$$

Each pair of differential measurements will result in a single estimate of the phase noise which is free from the effect of the ionospheric delay. The phase error can be estimated as a weighted average of all the differential measurements for each GNSS satellite in view, which results in

$$\tilde{\psi}_{uv,0}=\frac{2\pi}{\lambda_0}\cdot\left(\frac{\lambda_2^2}{\lambda_2^2-\lambda_1^2}\right)\cdot\sum_{i=1}^{N}\alpha_i\left[P_{Luv,1}^{(i)}-\left(\frac{\lambda_1}{\lambda_2}\right)^2\cdot P_{Luv,2}^{(i)}-\left(1-\frac{\lambda_1^2}{\lambda_2^2}\right)\cdot\tilde{\rho}_{uv}^{(i)}\right]-\frac{2\pi\cdot c}{\lambda_0}\cdot\delta\tilde{t}_{buv}. \tag{28}$$

Compared to the estimator given by (13), the one given by (28) is derived from half the number of measurements, and each measurement has a higher standard deviation. For the L1 and L2 frequencies from GPS (1575.42 and 1227.6 MHz, respectively), the final standard deviation of the estimation error will be multiplied by the factor

$$\frac{\sigma_{\text{ion-free}}}{\sigma_{\text{dual}}}=\sqrt{2}\cdot\frac{\sqrt{\lambda_2^4+\lambda_1^4}}{\lambda_1^2-\lambda_2^2}=4.20. \tag{29}$$

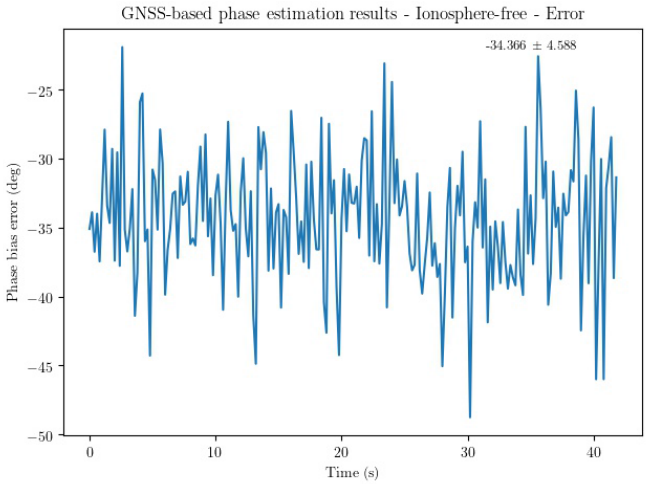

Fig. 8. Simulated phase drift data and results from GNSS-based phase error estimation.

Fig. 8 shows the estimation results applying the ionosphere-free phase error estimator. In the simulation, a difference of five total electron content unit (TECU) was introduced in the vertical total electron content (VTEC) between the two satellites. Carrier phase data from dual-frequency GPS receivers was simulated to enable estimation of the ionospheric delay. The remaining simulation parameters are shown in Table II.

By using the ionosphere-free algorithm, the standard deviation was increased by a factor of 2.9 compared to the results using a single-frequency receiver, which will be presented in detail in Section V. This ratio is still close to what predicts (29), since single-frequency receivers are expected to yield a phase error estimation with a standard deviation 1.41 higher than dual-frequency receivers, in the absence of high ionospheric delay differences. This multiplicative factor on the noise-like component of the estimation error is the penalty for estimating the ionospheric delay at each time step and corresponds to a worst-case scenario considering dual-frequency receivers. In case the ionospheric delay error remains approximately constant for the SAR integration time, or if it can be accurately interpolated from the POD solution, the previous estimator given by (13) is recommended, since it yields more precise results.

E. Unmodeled Components

Another error source in the GNSS measurement is the so-called phase center variation. Depending on the relative viewing geometry of the GNSS transmitter and receiver, the phase centers of the receiver and transmitter antenna vary. If this is not accounted for, it introduces an additional error to the phase measurement. This can be calibrated at a laboratory, as it was done in challenging minisatellite payload (CHAMP) and GRACE missions [24]. However, as remarked in [25], even after applying the laboratory calibration, other azimuth and elevation-dependent unmodeled variations persist. These errors can be further reduced by applying frequency-dependent patterns from on-orbit calibration, as demonstrated in [24]. They demonstrated that the carrier phase modeling is improved to a level of 4 mm, close to the pure receiver noise.

In the orbit determination process, the mean value of all the unmodelled errors cannot be separated from the GNSS receiver clock offset and, therefore, will bias it [23]. The effect of this error will cause a slight time offset, affecting the synchronization, and therefore will not affect considerably the positioning solution. For the application presented in this article, however, these effects are critical, and the biases must be calibrated to a value low enough so that they can be corrected in the data processing.

One of the potentially most critical error sources is the so-called multipath effect, which results from the superposition of the signal received directly from the GNSS satellite and the signal reflected by other surfaces. This error depends on the signal difference, the strength, and polarization of the reflected radiation, as well as the internal characteristics of the receiver [19]. The multipath effect is confined to a quarter of the navigation signal wavelength [26]. This can be a significant error, and the system must be designed to suppress or avoid it. For example, the two spacecraft used in the GRACE mission did not employ deployable solar panels, and their mechanical layout minimizes multipath effects. The PRISMA mission, which also performed experiments on POD, had the GPS antennas on the tips of the solar panels, which may have contributed to mitigating the problem of multipath effects. The strategy used in PRISMA is of particular relevance for low-cost SAR missions since their high power demand may require the use of deployable solar panels. On the other hand, this approach may introduce errors from residual solar panel vibrations and attitude uncertainties, which must be carefully evaluated and taken into consideration in early design trade-off studies.

The effect of multipath in the final phase estimation can be directly quantified from the corresponding component in (18), and it will consist of the weighted average of the contribution of each signal used in the estimation. The total multipath contribution to the synchronization error budget can be predicted by simulating the individual multipath errors, for example, through the procedure explained in [27], and applying the weighted averaging. One possible approach to mitigating multipath could be to identify the signals strongly affected by it and eliminate them from the estimation. Signals affected by multipath can be identified, for example, using the techniques detailed in [28] and [29].

In addition to the aforementioned errors, the phase measurements are affected by the so-called wind-up effect, which corresponds to the phase accumulation due to the rotation of the antennas about the mutual line-of-sight [19]. This error is not expected to be as significant as, for example, multipath errors, but it should also be considered.

F. Ambiguities

As shown in (18), errors in the ambiguity estimation for each signal will affect the final phase estimate. The constant phase channel biases also will bias carrier phase ambiguities [19]. This will have little effect on positioning, but it could be a relevant error source for an SAR application in which absolute phase reference is necessary. Having

absolute phase calibration independent of external data in the synchronization solution is relevant for specific applications. For interferometry, for example, having an absolute phase reference could make it possible to resolve the unknown ambiguity interval in the interferometric DEM without the need for height referencing on ground [14].

Since the ambiguities are constant for any given tracking arc, the corresponding error component will not change as long as the receiver remains locked to the same GNSS satellites during the SAR data acquisition time. This will most likely be the case for an acquisition time of a few minutes. If a GNSS satellite comes into view or goes out of view, using its carrier phase data may introduce a discontinuity into the relative phase estimate, which might appear masked in the estimated solution if inspected after averaging over navigation satellites.

The trivial but effective way to mitigate this problem would be to use only data from the GNSS satellites to which the receiver remains locked during the entire data acquisition period. This can result in discarding useful data for long acquisitions, but it is not expected to considerably degrade the performance of the technique because the satellites with visibility time of less than the short acquisition period will be few, and they will necessarily be seen at a low elevation, offering degraded measurements.

G. Long Versus Short Baseline Scenarios

Among the error contributions explained in Sections IV-A–IV-G, two are expected to degrade with the distance: the baseline error and the ionospheric delay. Considering that GRACE demonstrated submillimeter accuracy in baseline determination using only GNSS for a distance of around 220 km [30], we do not expect the accuracy of the PBD to be a performance driver at least up to that distance, and possibly beyond, assuming a GNSS receiver of comparable capabilities to the one used in GRACE. However, we expect the synchronization performance for long baselines to be considerably degraded by the decorrelation between the ionospheric effects on the carrier phases received at the two satellites. In [23], the authors evaluate the differential ionospheric delay on dual-frequency carrier phase measurements taken from the GRACE mission during a longitude swap maneuver, in which the satellites crossed at distances below 2 km. They concluded that the ionospheric delay was below carrier phase noise level for distances up to around 5 km. For longer distances, the effect of the differential ionospheric delays becomes apparent. As explained in Section IV-D, in principle, this effect could be eliminated through a linear combination of interfrequency carrier phase data at the cost of increased noise. Therefore, in principle, the technique could also be applied to distances up to 220 km but with a degraded performance.

In the case of companion missions, taking Harmony as an example, the transmitter could be at a distance of a couple of hundred kilometers from the receiver satellites, which could either be separated by a few hundred meters or by several hundreds of kilometers, depending on the mission phase [31]. The two Harmonies could be seamlessly synchronized using the GNSS-based synchronization technique presented here during the cross-track interferometric phase, in which the satellites will fly at a baseline of a few hundred meters in a helix configuration. The technique could also be applied for baselines of a couple of hundred kilometers if needed but with degraded performance.

As a final note, independently of the baseline, the applicability of the GNSS-based synchronization technique depends on the synchronization performance requirements, which depend on the radar carrier frequency and the particular application and must be evaluated individually.

V. System Example

This section provides an end-to-end simulation of the GNSS-based estimation for a C-band bistatic SAR using simple GNSS receivers. The purpose is to illustrate the potential of the suggested idea by providing an example of performance in a realistic environment. The parameters for the radars have been inspired by the ESA Earth Explorer 10 mission Harmony, which will consist of two companion passive-only satellites for Sentinel-1. The parameters for the positioning errors are based on results from the PRISMA mission [15] and the performance of the Phoenix GPS receiver by GSOC [21]. The error resulting from the orbit determination and the thermal noise is evaluated in the tested scenario. Fig. 9 shows the data flow and the major components of the simulation.

The simulation represents the two C-band bistatic SARs flying in close formation and with the suggested hardware configuration implemented. The navigation antennas on the radar spacecraft have direct visibility with nine GPS satellites during the simulation period. The orbits of all satellites are propagated using NASA's open-source software general mission analysis tool (GMAT) [32]. The software allows for the numerical integration of all orbits using an accurate gravitational model that includes drag and third-body attractions. The errors in the position and velocity of the radar satellites resulting from the POD have been simulated by introducing an absolute bias in the initial state of the satellites prior to orbit propagation. For convenience, historic GPS ephemerides are imported and propagated directly using the systems tool kit (STK) software.

After propagating the orbits, the ranges between the radar satellites and the GNSS satellites in view at a minimum elevation of 10° are calculated. The navigation raw data are simulated by adding the following error components to the expected code and phase signal: ionospheric delay, initial clock bias, thermal noise, and clock drift. The phase drift realization corresponds to a real measurement done with the synchronization link of TanDEM-X operated at a frequency of 3 kHz. The ionospheric delay is calculated assuming a background component only of a constant VTEC and applying the elevation-only-dependent mapping function by Lear [33]. In this case, even if simulated in the navigation raw data, the difference in the ionospheric delays affecting the signals in the satellites is negligible and was not considered in the phase estimator. A more complex scenario, including turbulence

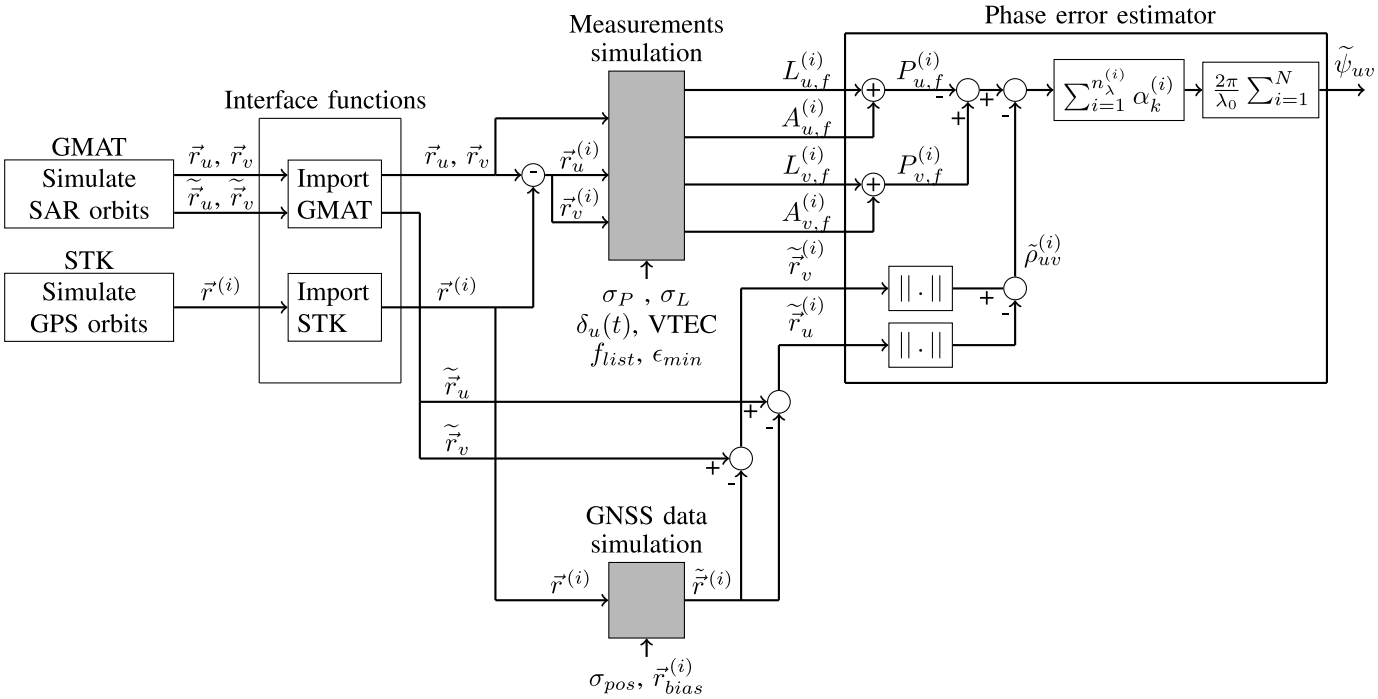

Fig. 9. Simulation framework used to test the proposed GNSS-based estimation of the radar carrier synchronization phase. GMAT stands for general mission analysis tool and STK for systems tool kit.

or bubbles, may benefit from the sensitivity of the different navigation carriers to the TEC variations.

The simulations assume the exploitation of only one frequency of the GNSS receiver (i.e., consistent with the Phoenix receiver), with noise characteristics in line with the Phoenix specification. The error figures are at the subcentimeter level, similar to those reported in the PRISMA mission, which also used a single-frequency GNSS receiver. The phase difference between the clocks is estimated using (13) with the weights as defined in (16). In the case of two-frequency receivers, the residuals of the estimation are expected to improve by a factor square root of two due to the availability of a second independent measurement, in addition to the improved accuracy due to a more accurate orbit determination, as discussed in Sections III and IV of this article. The ambiguity factors are assumed to be known from the POD process. Table II shows the simulation parameters and baseline errors.

Figs. 10 and 11 show the results of the simulation. As expected, the estimation of the oscillator phase error scaled to the radar carrier is biased but replicates the shape of the original error with a standard deviation below 2° for the simulation case. In Fig. 11, the estimation error presents a drift component-resulting in one 1° difference in the average error over the simulation period-caused by an error in the baseline velocity. This negligible phase ramp indicates that the technique could be used in applications where phase ramps due to oscillator signatures cannot be separated from the useful data (e.g., moving surface applications).

Under the assumptions of the simulation, the estimate may even be considered conservative since we considered a single-frequency receiver compatible with only one constellation. With hardware capable of receiving several constellations and

TABLE II
SIMULATION PARAMETERS

Parameter	Value
GNSS signal frequency	1575.42 MHz
Radar payload frequency	5405 MHz
Carrier phase standard deviation	0.0005 m
GNSS position bias standard deviation	1.5 m
Minimum elevation for visibility	10°
Number of GNSS satellites	9
Vertical Total Electron Content (VTEC)	50 TECU
Radial position error	1.478 m
Along-track position error	0.54 m
Across-track position error	-0.34 m
Radial velocity error	0.082 m/s
Along-track velocity error	0.010 m/s
Across-track velocity error	-0.007 m/s
Radial baseline error	8.248 mm
Along-track baseline error	1.177 mm
Across-track baseline error	0.767 mm
Radial baseline velocity error	0.0057 mm/s
Along-track baseline velocity error	-0.0077 mm/s
Across-track baseline velocity error	-0.0027 mm/s

several frequencies, the standard deviation may be reduced to below 1°. Note that not all systematic errors discussed in Section IV of this article have been included in the simulation because a more elaborated investigation is being planned in the scope of a follow-on research work using representative experimental data.

As discussed in Section IV, the effects due to multipath or upconverting electronics may be unavoidable and degrade the precision and accuracy of the solution. In case interferometric data are available, the integration of the suggested technique with a data-based synchronization algorithm (e.g., autosync) [10], [11], [34], [35] may be considered for the calibration of unmodeled error sources which do not remain constant

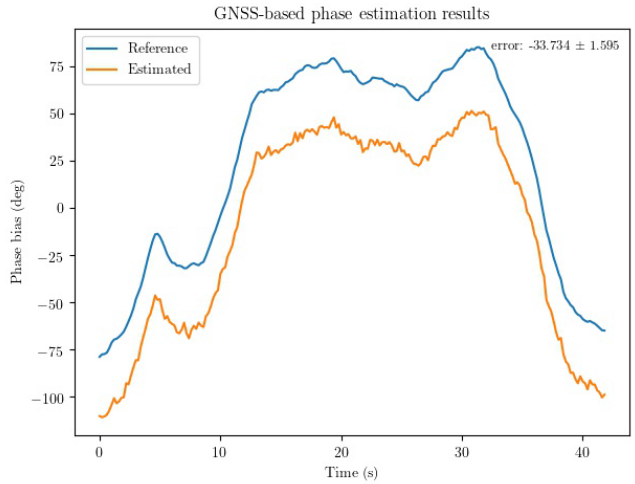

Fig. 10. Simulated phase drift data and results from GNSS-based phase error estimation.

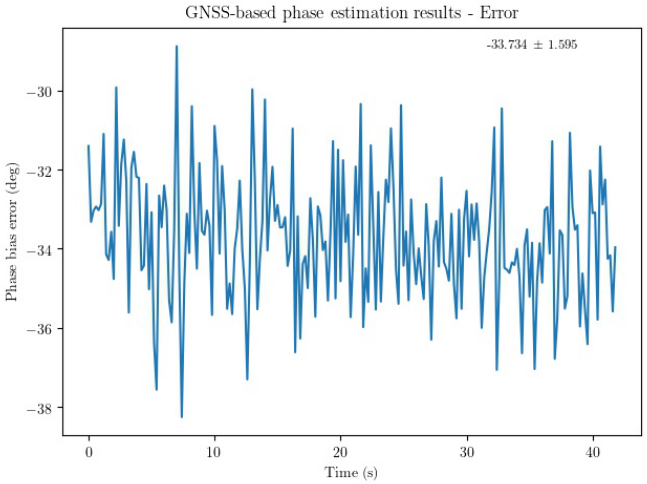

Fig. 11. Error in the GNSS-based phase estimation.

during the radar integration time, especially in the band of the clock phase errors. The simulation, however, indicates that the technique here presented would not have to rely on data-based synchronization and, therefore, would be suitable also for noninterferometric and moving surfaces applications. Last but not least, note the estimation model considered in this article does not make any assumption on the stochastic behavior of the radar clock. A better-suited estimator might reduce the estimation error even further.

VI. Conclusion

This article proposes an algorithm for phase synchronization considering a bistatic mission where, in each satellite, the radar payload and the GNSS receiver share the same oscillator. The phase error between the radar payloads can be derived from the differential carrier phase measurements provided by the GNSS receiver. Assuming that other error sources are either suppressed or compensated, the carrier phase measurement is affected by short-term phase noise variations of the oscillator and by the continuously changing geometry between the receivers and the GNSS satellite. The analysis indicates that the short variations in the carrier phase measurement due to phase noise from the oscillator can be isolated from the component due to geometric variations by using POD results since they vary at different time scales.

The technique presented here offers a simple solution for phase synchronization in bistatic or multistatic radar constellations. It has the potential for scalability since each additional satellite designed to employ the technique can be easily integrated into the multistatic system without adding to the complexity of the other elements of the space segment.

The simulations indicate that a standard deviation of 1.6° at C-band could be obtained from low-cost single-frequency GNSS receivers compatible only with the GPS constellation, assuming preservation of the phase signature of the oscillator within the radar payload and GNSS receiver, and only thermal noise as an error source. The solution relies on very precise relative navigation data. It assumes that the precision is in the subcentimeter level in relative precision and negligible in relative velocity. The performance can be improved considering the relatively recent widespread availability of navigation receivers compatible also with Galileo and BeiDou. The use of receivers operating with several frequencies is advised for the improvement of the phase accuracy and the calibration of ionospheric signatures, especially in scenarios with large baselines.

The error analysis indicates some critical issues that must be addressed for the technique to work. Of particular concern are multipath effects, which must be reduced to a minimum by carefully addressing the spacecraft design. The calibration of the upconverters must be carefully conducted to avoid inconsistent phase signatures in the estimated solution. Unlike using a synchronization link operated at the radar carrier, the errors of the GNSS-based estimation are expected to degrade-at least linearly-for increasing frequencies and could be at the edge of usability for X-band radar systems.

Future research work includes a validation of the error analysis of the proposed concept using a ground-based measurement setup simulating bi/multistatic SAR system configurations. In addition, the integration of the presented technique with others based on the data, such as autosync, could offer an improved solution and should be further assessed. Finally, it is important to investigate if the precision of the results from the GNSS-based estimator could be improved by smoothing techniques based on the stochastic behavior of the oscillator phase noise. Any eventual improvement could compensate for error sources not included in the model, thus making the concept more robust and viable.

References

[1] G. Krieger and A. Moreira, "Spaceborne bi- and multistatic synthetic aperture radar: Potential and challenges," *IEE Proc. Radar Sonar Navig.*, vol. 153, no. 3, pp. 184–198, Jun. 2006.

[2] J. L. Auterman, "Phase stability requirements for bistatic SAR," in *Proc. IEEE Nat. Radar Conf.*, Atlanta, GA, USA, Mar. 1984, pp. 48–52.

[3] N. Willis, *Bistatic Radar*. Norwood, MA, USA: Artech House, 1991.

[4] G. Krieger and M. Younis, "Impact of oscillator noise in bistatic and multistatic SAR," *IEEE Geosci. Remote Sens. Lett.*, vol. 3, no. 3, pp. 424–428, Jul. 2006.

[5] G. Krieger et al., "TanDEM-X: A satellite formation for high-resolution SAR interferometry," *IEEE Trans. Geosci. Remote Sens.*, vol. 45, no. 11, pp. 3317–3341, Nov. 2007.

[6] H. Braubach and M. Voelker, "Method for drift compensation with radar measurements with the aid of reference radar signals," U.S. Patent 7 209 072 B2, Apr. 24, 2007.

[7] M. Rodriguez-Cassola et al., "End-to-end performance analysis of companion SAR missions," in *Proc. IEEE Int. Geosci. Remote Sens. Symp. (IGARSS)*. Fort Worth, TX, USA: IEEE, Jul. 2017, pp. 153–156.

[8] G. Krieger, M. Zonno, J. Mittermayer, A. Moreira, S. Huber, and M. Rodriguez-Cassola, "MirrorSAR: A fractionated space transponder concept for the implementation of low-cost multistatic SAR missions," in *Proc. 12th Eur. Conf. Synth. Aperture Radar*. Aachen, Germany: VDE, Jun. 2018, pp. 1–6.

[9] J. Mittermayer et al., "MirrorSAR: An HRWS add-on for single-pass multi-baseline SAR interferometry," *IEEE Trans. Geosci. Remote Sens.*, vol. 60, pp. 1–18, 2022, Art. no. 5224018, doi: 10.1109/TGRS.2021.3132384.

[10] M. Rodriguez-Cassola et al., "First bistatic spaceborne SAR experiments with TanDEM-X," *IEEE Geosci. Remote Sens. Lett.*, vol. 9, no. 1, pp. 33–37, Jan. 2012.

[11] M. Rodriguez-Cassola, "Bistatic synthetic aperture radar data processing," Ph.D. dissertation, Inst. Radio Freq. Eng. Electron. (IHE), Karlsruhe Inst. Technol. (KIT), Karlsruhe, Germany, 2012.

[12] W.-Q. Wang, "GPS-based time & phase synchronization processing for distributed SAR," *IEEE Trans. Aerosp. Electron. Syst.*, vol. 45, no. 3, pp. 1040–1051, Jul. 2009.

[13] R. Kroes, O. Montenbruck, W. Bertiger, and P. Visser, "Precise GRACE baseline determination using GPS," *GPS Solutions*, vol. 9, no. 1, pp. 21–31, Apr. 2005.

[14] J. H. González et al., "Bistatic system and baseline calibration in TanDEM-X to ensure the global digital elevation model quality," *ISPRS J. Photogramm. Remote Sens.*, vol. 73, pp. 3–11, Sep. 2012.

[15] J.-S. Ardaens, S. D'Amico, and O. Montenbruck, "Flight results from the PRISMA GPS-based navigation," in *Proc. 5th ESA Workshop Satell. Navigat. Technol. (NAVITEC)*, Noordwijk, The Netherlands, Jan. 2010, pp. 8–10.

[16] G. Krieger and F. De Zan, "Relativistic effects in bistatic SAR processing and system synchronization," in *Proc. 9th Eur. Conf. Synth. Aperture Radar*, Apr. 2012, pp. 231–234.

[17] P. van Barneveld, "Orbit determination of satellite formations," Ph.D. dissertation, Fac. Aerosp. Eng., Delft Univ. Technol., Delft, The Netherlands, 2012.

[18] S. J. Setty, P. J. Cefola, H. Fiedler, and J. F. S. J. Diaz, "Attributes affecting the accuracy of a batch least square orbit determination using semi-analytical satellite theory," in *Proc. Maui Opt. Space Surveill. Technol. Conf.*, Sep. 2016, p. 116.

[19] R. Kroes, "Precise relative positioning of formation flying spacecraft using GPS," Ph.D. dissertation, Dept. Space Eng., Delft Univ. Technol., Delft, The Netherlands, 2006.

[20] P. D. Groves, *Principles of GNSS, Inertial, and Multisensor Integrated Navigation Systems*. Norwood, MA, USA: Artech House, 2013.

[21] O. Montenbruck and C. Renaudie, "Phoenix-S/-XNS performance validation," German Space Oper. Center (GSOC) Deutsches Zentrum für Luft- und Raumfahrt (DLR) e.V., Weßling, Germany, DLR Tech. Rep. GTN-TST-0120, Apr. 2007.

[22] U. Weinbach, S. Schon, and T. Feldmann, "Evaluation of state-of-the-art geodetic GPS receivers for frequency comparisons," in *Proc. IEEE Int. Freq. Control Symp. Joint 22nd Eur. Freq. Time Forum*, Apr. 2009, pp. 263–268.

[23] O. Montenbruck, P. vanBarneveld, Y. Ysoon, and Visser, "GPS-based precision baseline reconstruction for the TanDEM-X SAR-formation," in *Proc. 19th Int. Symp. Space Flight Dyn.*, Annapolis, MD, USA, Sep. 2007.

[24] O. Montenbruck, M. Garcia-Fernandez, Y. Yoon, S. Schön, and A. Jäggi, "Antenna phase center calibration for precise positioning of LEO satellites," *GPS Solutions*, vol. 13, no. 1, pp. 23–34, Jan. 2009.

[25] A. Jäggi, R. Dach, O. Montenbruck, U. Hugentobler, H. Bock, and G. Beutler, "Phase center modeling for LEO GPS receiver antennas and its impact on precise orbit determination," *J. Geodesy*, vol. 83, no. 12, pp. 1145–1162, Jul. 2009.

[26] B. Hofmann-Wellenhof, H. Lichtenegger, and J. Collins, *GPS, Theory and Practice*. New York, NY, USA: Springer-Verlag Wien, 1997.

[27] L. Lau and P. Cross, "Development and testing of a new ray-tracing approach to GNSS carrier-phase multipath modelling," *J. Geodesy*, vol. 81, no. 11, pp. 713–732, Oct. 2007.

[28] P. R. R. Strode and P. D. Groves, "GNSS multipath detection using three-frequency signal-to-noise measurements," *GPS Solutions*, vol. 20, no. 3, pp. 399–412, Jul. 2016.

[29] N. Kubo, K. Kobayashi, and R. Furukawa, "GNSS multipath detection using continuous time-series C/N0," *Sensors*, vol. 20, no. 14, p. 4059, Jul. 2020.

[30] X. Guo and Q. Zhao, "M-estimation-based robust and precise baseline determination for formation-flying satellites," *GPS Solutions*, vol. 25, no. 2, pp. 1–12, Apr. 2021.

[31] J. Lopez-Dekker et al., "The Harmony mission: Applications and preliminary performance," in *Proc. 6th Workshop Adv. RF Sensors Remote Sens. Instrum. (ARSI)*, vol. 19, 2019, pp. 1–6.

[32] *General Mission Analysis Tool (GMAT) Project Page*. Accessed: Oct. 2020. [Online]. Available: https://opensource.gsfc.nasa.gov/projects/GMAT/index.php

[33] W. Lear, "GPS navigation for low-earth orbiting vehicles," NASA Lyndon B. Johnson Space Center, Mission Planning Anal. Division, Washington, DC, USA, Tech. Rep. NASA 87-FM-2, JSC-32031, rev. 1, 1987.

[34] H. Cantalloube, M. Wendler, V. Giroux, P. Dubois-Fernandez, and G. Krieger, "Challenges in SAR processing for airborne bistatic acquisitions," in *Proc. EUSAR*, 2004, pp. 577–580.

[35] H. Cantalloube, P. Dubois-Fernandez, V. Giroux, and G. Krieger, "Bistatic moving target indication using across-track and along-track interferometry," in *Proc. EUSAR*, 2006, pp. 1–4.

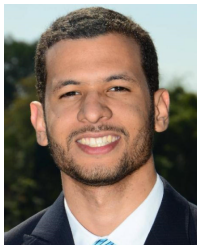

Eduardo Rodrigues-Silva was born in Imperatriz, Brazil, in 1991. He received the B.Sc. degree in aerospace engineering from the Aeronautical Technological Institute (ITA), São José dos Campos, Brazil, in 2014, and the M.Sc. degree in aerospace engineering from the Technical University of Berlin, Berlin, Germany, in 2019.

From 2015 to 2017, he worked as a Space System Engineer at Visiona Tecnologia Espacial, in São José dos Campos. Since 2019, he has been working towards the Ph.D. degree with the Karlsruhe Institute of Technology, Karlsruhe, Germany. He has been with the Microwaves and Radar Institute, German Aerospace Center (DLR-HR), Weßling, Germany, as a Ph.D. Student, since 2019. His current research interests include synchronization for bistatic and multistatic SAR, formation flying, and the study of distributed systems architectures for spaceborne radar remote sensing.

Marc Rodriguez-Cassola was born in Barcelona, Spain, in 1977. He received the Ingeniero degree in telecommunication engineering from the Universidad Pública de Navarra, Pamplona, Spain, in 2000, and the Licenciado (M.Sc.) degree in economics from the Universidad Nacional de Educación a Distancia, Madrid, Spain, in 2012, and the Ph.D. degree in electrical engineering from the Karlsruhe Institute of Technology, Karlsruhe, Germany, in 2012.

From 2000 to 2001, he was a Radar Hardware Engineer with the Study Center of Terrestrial and Planetary Environments (CETP)/French National Center for Scientific Research (CNRS), Saint Maur des Fosses, France. From 2001 to 2003, he was a Software Engineer with Altran Consulting, Munich, Germany. Since 2003, he has been with German Aerospace Center, Microwaves and Radar Institute, Weßling, Germany, where he is leading the SAR Missions Group. His research interests include radar signal processing, SAR end-to-end simulation, SAR processing and calibration algorithms, crisis theory, and radar mission analysis and applications.

Gerhard Krieger (Fellow, IEEE) received the Dipl.-Ing. (M.S.) and Dr.-Ing. (Ph.D.) degrees (Hons.) in electrical and communication engineering from the Technical University of Munich, Munich, Germany, in 1992 and 1999, respectively.

From 1992 to 1999, he was with the Ludwig Maximilians University, Munich, where he conducted multidisciplinary research on neuronal modeling and nonlinear information processing in biological and technical vision systems. Since 1999, he has been with the Microwaves and Radar Institute of the German Aerospace Center (DLR), Weßling, Germany, where he started as a Research Associate developing signal processing algorithms for a novel forward-looking radar system employing digital beamforming on receive. From 2001 to 2007, he led the New SAR Missions Group, which pioneered the development of advanced bistatic and multistatic radar systems, such as TanDEM-X, as well as innovative multichannel SAR techniques and algorithms for high-resolution wide-swath SAR imaging. Since 2008, he has been the Head of the Radar Concepts Department which currently hosts about 50 scientists focusing on new SAR techniques, missions, and applications. He has been serving as a Mission Engineer for TanDEM-X and he made major contributions to the development of the Tandem-L mission concept, where he led the Phase-0 and Phase-A studies. Since 2019, he holds professorship at the Friedrich-Alexander-University Erlangen, Erlangen, Germany, and he has authored or coauthored more than 100 peer-reviewed journal articles, nine invited book chapters, about 500 conference papers, and more than 20 patents.

Prof. Krieger served as the Technical Program Chair for the European Conference on Synthetic Aperture Radar in 2014. He received several national and international awards, including two Best Paper Awards at the European Conference on Synthetic Aperture Radar, two Transactions Prize Paper Awards of the IEEE Geoscience and Remote Sensing Society, and the W.R.G. Baker Prize Paper Award from the IEEE Board of Directors. He has been an Associate Editor for IEEE TRANSACTIONS ON GEOSCIENCE AND REMOTE SENSING since 2012. He served as a Guest Editor for IEEE JOURNAL OF SELECTED TOPICS IN APPLIED EARTH OBSERVATIONS AND REMOTE SENSING.

Alberto Moreira (Fellow, IEEE) received the bachelor's and master's degrees in electrical engineering from the Aeronautical Technological Institute (ITA), São José dos Campos, Brazil, in 1984 and 1986, respectively, and the Ph.D. degree (Hons.) from the Technical University of Munich, Munich, Germany, in 1993.

From 1996 to 2001, he was the Head of the Synthetic Aperture Radar (SAR), Technology Department, German Aerospace Center (DLR), Oberpfaffenhofen, Germany. Under his leadership, the DLR airborne SAR system has been upgraded to operate in innovative imaging modes like polarimetric SAR interferometry, tomography and holography. Since 2001. He is the Director of the Microwaves and Radar Institute, DLR, and a Professor with the Karlsruhe Institute of Technology (KIT), in the field of microwave remote sensing. His DLR's Institute contributes to several scientific programs and projects for spaceborne SAR missions like TerraSAR-X, TanDEM-X, SAR-Lupe, and SARah, as well as Kompsat-6, PAZ, Sentinel-1, BIOMASS, ROSE–L, Harmony, Sentinel-1NG, Envision, and VERITAS. The mission TanDEM-X, led by his Institute, has generated a global, high-resolution digital elevation model of the Earth with unprecedented accuracy. He is the Initiator and Principal Investigator (PI) for this mission. He has served as a member for the ESA Mission Advisory Groups of ENVISAT/ASAR, Sentinel-1, and Hydroterra, and is currently serving as a member of the Science Study Team for the ESA's mission EnVision. He is author or co-author of more than 500 publications in international conferences and journals, eight book chapters, and holds more than 45 international patent grants in the radar and antenna field. His professional interests and research areas encompass spaceborne radar end-to-end system design, microwave techniques and system concepts, signal processing, and remote sensing applications.

Prof. Moreira is recipient of several international awards including the IEEE Aerospace and Electronic Systems Society (AESS), Fred Nathanson Award in 1999, the IEEE Kiyo Tomiyasu Technical Field Award in 2007, IEEE W.R.G. Baker Award from the IEEE Board of Directors in 2012, the IEEE GRSS Distinguished Achievement Award in 2014, and the IEEE Dennis J. Picard Medal for Radar Technologies and Applications in 2023. He and his colleagues received the GRSS Transactions Prize Paper Awards in 1997, 2001, and 2007, and the GRSS Letters Prize Paper Award in 2015 and 2017. He has served as a President of the IEEE Geoscience and Remote Sensing Society (GRSS) in 2010, as well as a General Co-Chair of IGARSS in 2012, and General Chair of EUSAR in 2006. He was the Founder and Chair of the GRSS German Chapter from 2003 to 2008, he served as an Associate Editor for the IEEE GEOSCIENCE AND REMOTE SENSING LETTERS from 2003 to 2007, and for the IEEE TRANSACTIONS ON GEOSCIENCE AND REMOTE SENSING since 2005, and he has been serving as a Chair of the Major Awards of GRSS since 2017.